

www.acsanm.org Article

Two-Dimensional Quantum-Confined CsPbBr₃ in Silicene for LED Applications

Roberto Gonzalez-Rodriguez, Evan Hathaway, Holden Paulette, Jeffery L. Coffer, Yuankun Lin, and Jingbiao Cui*



Cite This: ACS Appl. Nano Mater. 2023, 6, 4028-4033



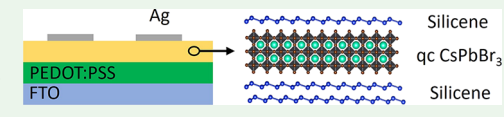
ACCESS I

III Metrics & More

Article Recommendations

s Supporting Information

ABSTRACT: Perovskites with reduced dimensions are very attractive for LED applications due to their improved stability and efficient energy transfer. This is exemplified by 2D perovskites reported in the literature, predominantly either Dion-Jacobson or Ruddlesden—Popper systems, which typically use long chain alkyl moieties as spacers in order to form 2D layers. Here, we report an approach



which uses an inorganic 2D material—silicene—as a template to form two-dimensional quantum-confined CsPbBr₃ (qc-CsPbBr₃) layers of less than 5 nm in thickness. This approach can be further generalized to synthesize other types of perovskites with reduced dimensionality. The structural and optical properties of the qc-CsPbBr₃ layers inside silicene were characterized. The qc-CsPbBr₃-based LEDs demonstrate improved stability under ambient conditions, along with a current efficiency of 13.7 Cd A⁻¹ and external quantum efficiency of 8.5%.

KEYWORDS: silicene, 2D material, perovskites, LEDs, quantum confinement

INTRODUCTION

Perovskites have attracted much attention in recent years due to their useful properties such as high charge carrier mobility, 1-4 high dielectric constant, 5 and processability, making them uniquely suitable for applications in photovoltaics, light emitting diodes (LEDs), lasers, and photodetectors.⁶⁻⁹ Most perovskites reported in the literature are found in either thin film or bulk material morphologies; however, recent studies have shown that the physical properties of 2D perovskites are more easily tuned when compared to these other two morphologies. Structural control in such 2D perovskites is typically limited by the selection of the identity of a long alkyl chain. 10 Stable exciton states with unusually high binding energies are found in 2D perovskites even at room temperature due to the confinement of electrons and holes within the thin perovskite layers. 11 This leads to an increase in the electron-hole recombination, thus making 2D perovskites ideal for LED applications.¹²

Most 2D perovskites reported in the literature are formed with the addition of a large cation, usually organic, with a very long alkyl chain which cannot enter the octahedron spaces and thus limits the growth along the out of plane direction. The 2D perovskites fabricated using this method have a generic formula, $RA_{n-1}BX_{3n-1}$ or (Ruddlesden–Popper series), where A is the cation (A = Methylammonium (MA), Formamidinium (FA) or Cesium (Cs)), B is Lead (Pb) or Tin (Sn), X is the halogen (X = Cl, Br, and I)), and R is the spacer between the perovskite layers. The R group can be an aliphatic or aromatic alkylammonium cation, of which the most commonly used are butylamine (BA⁺ = CH₃(CH₂)₃NH₃) and phenethylamine (PEA, C₆H₅C₂H₄NH₃), respectively. This 2D system

acts as multiple quantum wells with the R layer serving as a potential barrier between the 2D perovskite layers. ^{15,16} The Dion-Jacobson system is another type of 2D perovskite, in which the R spacer between the perovskite layers is a divalent cation, such as ethylenediamine or 1,4-butanediamine. ¹⁷

Current research has shown that the cation-containing spacer layer is key to the formation and stabilization of 2D perovskites. In this study, we, for the first time, obtained twodimensional quantum-confined CsPbBr₃ (qc-CsPbBr₃) ultrathin layers sandwiched inside 2D silicene (i.e., silicon nanosheets) by using silicene as a template. It is well-known that silicene is a single 2D layer of silicon nanosheets analogous to graphene. The morphological and structural properties of qc-CsPbBr3 were studied using X-ray diffraction (XRD), transmission electron microscopy (TEM), and energy dispersive X-ray spectroscopy (EDX). The sandwiched perovskite nanosheets show significantly improved stability in air. Photoluminescence (PL) and electroluminescence (EL) of the quantum-confined perovskite-based LEDs show stable light emission over 8 weeks, demonstrating a great improvement over unstable emission from their bulk analogs.

Received: January 30, 2023 Accepted: February 9, 2023 Published: February 21, 2023





RESULTS AND DISCUSSION

We have previously produced silicene through an exfoliative process, using CaSi₂ as a starting material. In short, this process consists of the removal of Ca from CaSi₂ using HCl, followed by sonication and centrifugation, after which the silicene are dried and stored in vacuum for use. Figure S1 shows XRD patterns of the starting material, CaSi₂, and silicene after exfoliation and confirms that silicene layers were indeed obtained. Scanning electron microscopy (SEM) images of the CaSi₂ and silicene are shown in Figure S2. Here, it can be seen that the removal of Ca from CaSi₂ leaves a layered silicon structure, which can then be used as a template for perovskite growth with reduced dimensionality. Figure 1a

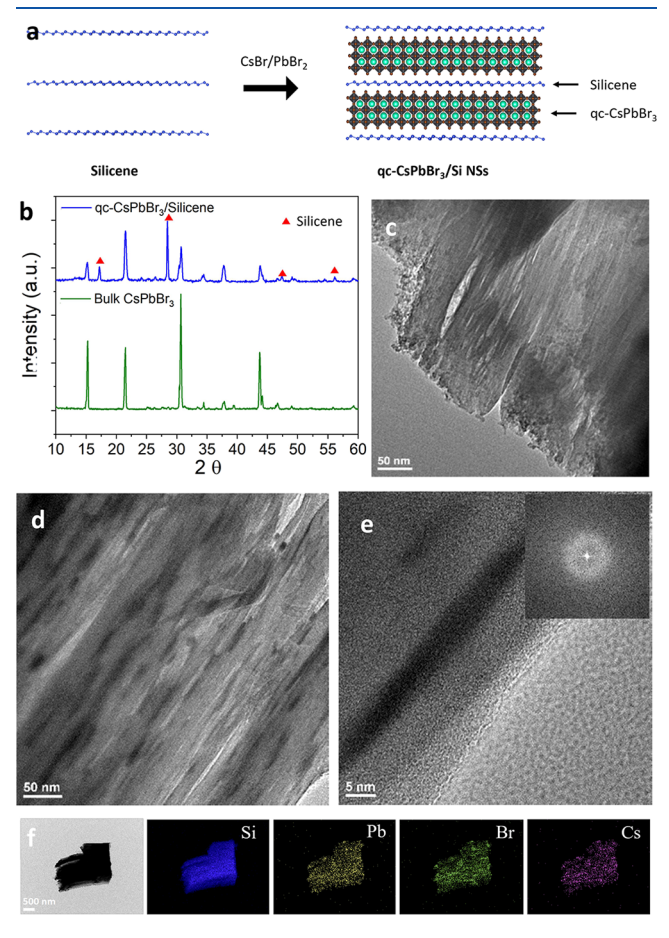


Figure 1. (a) Schematic representation of the silicene template and qc-CsPbBr₃ in silicene; (b) XRD of qc-CsPbBr₃ in silicene and bulk CsPbBr₃; (c) TEM image of the silicene template; (d) TEM image of qc-CsPbBr₃ in silicene; (e) TEM image of an individual qc-CsPbBr₃ layer in silicene; and (f) TEM-EDX map of qc-CsPbBr₃ in silicene.

shows a schematic diagram for the templated growth of quantum-confined perovskites. The perovskite infiltration process begins with the immersion of the silicene template in a solution containing the perovskite precursors CsBr and CsPbBr₂ in a 1:1 mole ratio, followed by a separation process using centrifugation and ending with the samples being baked at 95 °C for 30 min.

Figure 1b shows XRD patterns for bulk CsPbBr₃ and for qc-CsPbBr₃ in silicene. Bulk CsPbBr₃ XRD peaks are located at 15.2° , 22.1° , 26.4° , 30.6° , 34.3° , 37.7° , 43.9° , and 46.8° and can be assigned to the (100), (110), (111), (200), (210), (211), (220), and (300) planes of CsPbBr₃, respectively. A

typical SEM image for bulk $CsPbBr_3$ is shown in Figure S3. ^{21,22} The XRD spectrum for qc-CsPbBr₃ shows peaks, which are consistent with those seen in bulk $CsPbBr_3$ along with a few additional peaks, which are associated with the silicene template. The perovskite-associated peaks from qc-CsPbBr₃ are broader than those of the bulk material due to nanoscale thin layers.

Figure 1c,d shows TEM images of the silicene template and the qc-CsPbBr₃ in silicene respectively. Before infiltration, empty gaps can be seen between the silicene layers of the template (Figure 1c). After perovskite infiltration, the empty gaps between silicene layers are filled with CsPbBr₃ as demonstrated by the dark regions representing the thin CsPbBr₃ sandwiched between the lighter silicene layers (Figure 1d,e). The thickness of the two-dimensional quantum-confined perovskite layers is less 5 nanometers. In order to verify the uniformity of perovskite infiltration between the silicene layers, a TEM-EDX map was performed and is shown in Figure 1f. The distribution of elements associated with the perovskite composition, that is, Cs, Pb, and Br matches that of silicon and is consistent with the uniform formation of ultrathin perovskite nanostructures confined between the silicene nanosheets.

The absorption spectrum for qc-CsPbBr₃ in silicene is shown in Figure S4. The PL spectra from the bulk and qc-CsPbBr₃ in silicene were taken using a laser with an excitation wavelength of 375 nm and are shown in Figure 2. The inset of

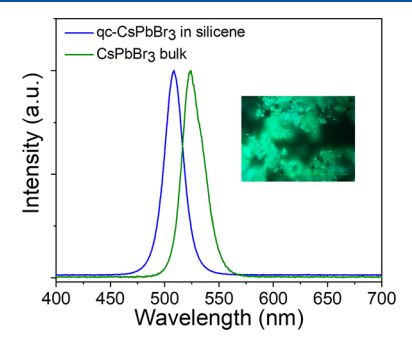


Figure 2. Normalized PL spectrum of bulk and qc-CsPbBr₃ in silicene. (Inset: PL image from qc-CsPbBr₃ in silicene).

Figure 2 shows the corresponding PL image of qc-CsPbBr₃ in silicene, while the typical PL image for bulk CsPbBr3 is shown in Figure S5. A peak shift from 507 nm for qc-CsPbBr3 in silicene to 523 nm for bulk CsPbBr₃ is observed. The blue shift of the PL peak in qc-CsPbBr₃ is most likely due to the quantum confinement of the electrons within the twodimensional layers, although charge transfer between the silicene layers and ultrathin CsPbBr3 might also affect PL emission. If the PL shift is related purely to a quantum confinement effect, then the peak energy E for the confined perovskite can be written as $E = E_g + b/r^2$, where E_g is the band gap for the bulk perovskite, r is the perovskite thickness, and bis a constant with a value of 2.6 eV nm² for CsPbBr₃.^{23,24} By taking the PL maxima as the optical band gaps E and E_{σ} of the confined and bulk CsPbBr₃ respectively, the average thickness (r) is estimated to be about \sim 8 nm, which is equivalent to \sim 10 layers of CsPbBr₃. This value is close to the thickness obtained in our TEM measurements. The single PL peak from qc-CsPbBr₃ suggests that the perovskite loading into the template does not produce bulk residues inside or outside the silicene layers.

The stability of qc-CsPbBr₃ in silicene was studied by XRD and PL measurements over the course of 2 months. For comparison, the XRD and PL spectra of bulk CsPbBr₃ were also measured over the same period of time and are shown in Figure 3a,b, respectively. Figure S6 shows the XRD spectrum

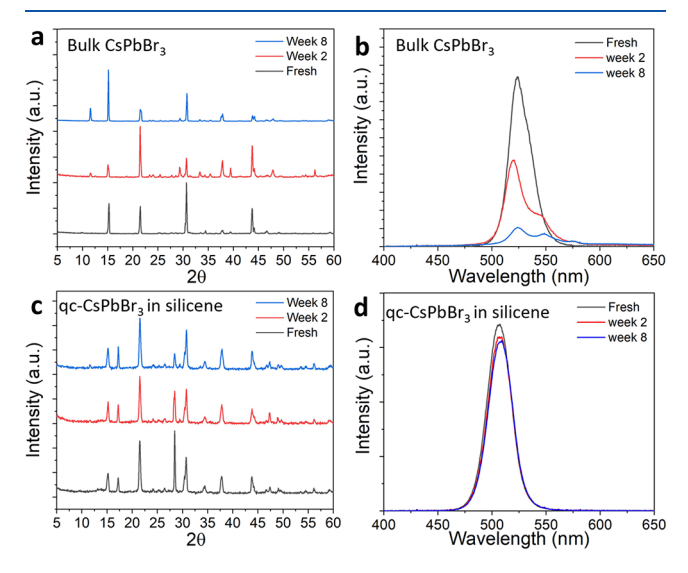


Figure 3. Stability study of $CsPbBr_3$ after storage for different times under ambient conditions. (a) XRD and (b) PL spectra of bulk $CsPbBr_3$; and (c) XRD and (d) PL spectra of quantum-confined $CsPbBr_3$ in silicene.

of the Si wafer substrate. The fresh bulk perovskite sample shows the typical XRD peaks as expected for CsPbBr3. However, after storage under ambient conditions for 2 weeks a new peak at $\sim\!11.5^{\circ}$ is observed. This diffraction peak is due to the phase transformation and degradation of CsPbBr3 into CsPb2Br5 as a result of moisture incorporation into the crystal lattice. This is consistent with the reported instability of CsPbBr3 in air and was previously observed in CsPb2Br5 synthesized using different ratios of PbBr2 and CsBr in water. The PL spectrum taken after 2 weeks (see Figure 3b) shows a decreased intensity along with two emission peaks due to the mixture of CsPbBr3 and CsPb2Br5. After 8 weeks in air, the PL intensity further decreases and more peaks are observed. As expected, this result again demonstrates the instability of the bulk CsPbBr3 under ambient conditions.

Figure 3c shows the XRD patterns from qc-CsPbBr₃ in silicene up to 8 weeks after preparation. Unlike the bulk sample, the confined perovskite sample does not show any obvious signs of degradation even after aging for 8 weeks. This demonstrates the stability improvement of qc-CsPbBr₃ due to the reduced dimensionality of the perovskite. The protection of silicene might also play a role in stability improvement; however, a slow degradation usually occurs under protection. Figure 3d shows the PL spectra of qc-CsPbBr₃ in silicene. After the sample was stored in air for 2 weeks, the PL intensity decreases slightly. After this initial decrease, the PL spectra are stable for the remainder of the time, once again indicating that the quantum-confined perovskites in silicene are highly stable.

The stability of qc-CsPbBr $_3$ in silicene coated with a protection layer of 15 nm Al $_2$ O $_3$ was also studied. Figures S7 shows PL intensity change over time for the unprotected and Al $_2$ O $_3$ -protected qc-CsPbBr $_3$ in silicene, and Figure S8 shows the corresponding XRD spectra. The sample coated with the

Al₂O₃ protection layer shows only a very slight improvement in the PL stability over time. Both the XRD and PL studies show that qc-CsPbBr₃ silicene is very stable.

The LED devices based on qc-CsPbBr₃ in silicene were fabricated on FTO glass substrates. The device architecture consists of a layer of poly(3,4-ethylene dioxythiophene):poly(styrene sulfonate), also known as PEDOT:PSS, as a hole transport layer, qc-CsPbBr₃ in silicene on top of PEDOT:PSS, silver as the top electrode, and FTO as the back electrode. The cross-sectional SEM image of the device is shown in the inset of Figure 4c, which clearly shows the FTO and CsPbBr₃ layers.

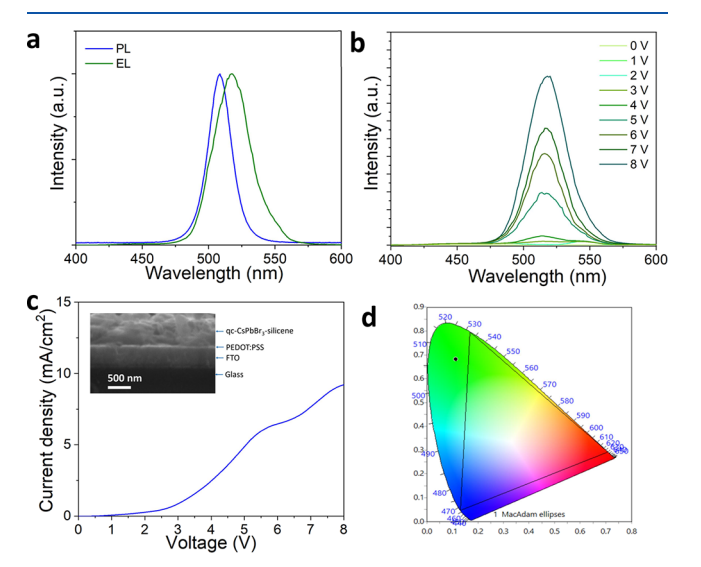


Figure 4. (a) Normalized PL and EL of the quantum-confined CsPbBr₃ in silicene; (b) EL spectra measured at different applied voltages; (c) current–voltage plot of the LED device (inset: SEM-device cross-section); (d) Commission Internacionale de l'Eclairage (CIE) chromaticity coordinates.

PEDOT:PSS is hard to distinguish in the image because the polymer has small contrast and its thickness is only around 65 nm. The holes injected from the hole transport material, PEDOT:PSS, and the electrons from the Ag electrode come into the recombination layer of CsPbBr₃ in siliene, where the electrons and holes recombine to release energy in the form of photons.

Figure 4a shows the measured PL and EL spectra at 7 V for qc-CsPbBr3 in silicene. Note that the EL peak position is at 517 nm, while the PL peak position is at 507 nm. This shift in emission peak can be attributed to the fluctuation of the interfacial states at the PEDOT:PSS layer and the band bending between PEDOT:PSS and qc-CsPbBr3 in silicene. 29 31 The exact same cause also results in the broadening of the EL peak. For comparison, an LED based on bulk CsPbBr3 in the same device architecture was also fabricated and studied. The EL emission for this bulk CsPbBr3 device exhibits an EL peak at 532 nm as shown in Figure S9. This represents a peak position shift of 9 nm between PL and EL for the bulk CsPbBr₃, which is similar to that of 10 nm shift for qc-CsPbBr₃. It is noted that the EL peak position difference between bulk and the confined CsPbBr3 is 15 nm, which is similar to the observed peak position difference of 16 nm in PL due to quantum confinement.

Figure 4b shows the electroluminescence spectra of the LED device measured at different applied voltages while the inset

Table 1. Comparison of LED Devices Based on Perovskites

device structure	λ_{EL} peak (nm)	CE (cd/A)	EQE (%)	T_{50} stability	ref
ITO/poly-TPD/PFN/(PEA) ₂ Cs _n Pb _n Br _{3n+1} /TPBi/LiF/Al	512	45.2	14.4	~25 min-3.5 V	35
$ITO/PEDOT:PSS/(PEA)_2MA_{n-1}Pb_nBr_{3n+1}/TPBi/LiF/Al$	526		7.4		36
$ITO/PEDOT:PSS/(PEOA)_2MA_{n-1}Pb_nBr_{3n+1}/TPBi/Ba/Al$	494	2.1	1.1		37
$ITO/PEDOT:PSS/PFNBr/(p-FPEA)_2MA_{n-1}Pb_nBr_{3n+1}/PMMA/TmPyPB/LiF/Al$	525		12.1	203 s	38
$ITO/PEDOT:PSS/PA_2Cs_{n-1}Pb_nBr_{3n+1}/TmPyPB/Cs_2CO_3/Al$	505	7.32	3.6	30 min-4.8 V	39
$ITO/NiO_x/(BA)_2FA_2Pb_3Br_{10}/TPBi/LiF/Al$	540	62.4	14.6	102 min	40
$ITO/PEDOT:PSS/CBP/(OLA)_2MA_{n-1}Pb_nBr_{3n+1}/TPBi/LiF/Al$	492		0.23		41
FTO/PEDOT:PSS/qc-CsPbBr ₃ /Ag	518	13.7	8.5	~40 min	this work

shows the plots of the EL intensity vs the applied voltage. It is hard to observe the EL emission at voltages below 3 V. As the applied voltage increases above 3 V, the EL intensity increases quickly, while the EL peak shape stays the same, indicating that the quantum-confined perovskite is stable under an applied electric field. The turn-on voltage for EL emission is consistent with the current density increase with the measured electric current increasing slowly at voltages lower than 3 V, and then, it increases relatively steeply above 3 V as shown in Figure 4c. Figure 4d shows the Comission Interationale de l'Eclairage (CIE) chromaticity coordinates, including our data at (0.113, 0.681). It is located in the pure green region, making the CsPbBr₃ ideal for pure green light-emitting sources. The triangle in Figure 4d represents the chromaticity standard for ultra-high-definition television UHD TV (ITU-R BT 2020).

Table 1 lists the performance of a number of perovskite LED devices from the literature as well as the data from the quantum confined perovskites in this study. The details of the device structures and the types of perovskite materials are also included in the table. To ensure a valid comparison, only the devices with green emission are selected. The perovskite devices in this study show a competitive external quantum efficiency (EQE) and stability with a moderate CE. The EQE shown in the table for this student was obtained by using the ratio of emitted photons to the injected electrons based on the current at 7 V. The EQE %, CE, and luminance vs current density are shown in Figure S10. The PL lifetime au was measured for both bulk CsPbBr3 and qc-CsPbBr3 in silicene with values of 3.6 and 5.5 ns, respectively (see Figure S12). The longer lifetime shows a better exciton confinement, inhibiting the trapping of the excited electrons by surface defects and resulting in an efficient usage of the excited carriers in the confined perovskite than the bulk materials. The improved emitting properties in qc-CsPbBr3 is associated with the quantum confinement effect, which is consistent with the literature. 32-34 More efforts are needed to systematically study the dependence of lifetime on the confined layer thickness in order to have a better understanding of the underlying physics. The performance of these two-dimensional quantum-confined perovskite devices may be further improved by adding layers such as LiF and NiO as reported in refs 35, 37, 38.

CONCLUSIONS

In this study, we used 2D silicene as a template to fabricate two-dimensional quantum-confined perovskite of CsPbBr₃. The TEM and PL data show that the perovskites were confined between the 2D silicene layers with a thickness of less than 5 nanometers. The XRD and PL measurements confirm that the stability of the quantum-confined CsPbBr₃ in silicene was significantly improved as compared to the bulk material. We demonstrate that the confined CsPbBr₃ in silicene has

potential applications in light-emitting devices with a EQE of 8.5% and a CE of 13.7 Cd/A. The template-assisted process can be further generalized to the synthesis of other types of confined perovskites.

EXPERIMENTAL METHODS

Materials and Equipment. The chemicals and materials that were purchased from Sigma-Aldrich include dimethyl sulfoxide (DMSO), calcium silicide (CaSi₂), lead bromide (PbBr₂), and cesium bromide (PbBr₂). Poly(3,4-ethylene dioxythiophene):poly(styrene sulfonate) (PEDOT:PSS) were purchased from Polyscience. All the materials were used as received without further purification.

Characterization was done with scanning electron microscopy (SEM, FEI Quanta 200 and JEOL-JSM-7100F), transmission electron microscopy (TEM, JEOL JEM-2100), X-ray diffraction (XRD, Rigaku Ultima III). Electrical characterization was measured by a Keithley 4200 semiconductor analyzer. Photoluminescence (PL) spectroscopy and images were taken using a Nikon fluorescence microscope with an excitation wavelength of 375 nm.

2D Silicene Synthesis and Perovskite Loading. CaSi $_2$ (0.5 g) was kept for 3 days in HCl at $-10~^{\circ}$ C under continuous stirring. The Si ML product was separated by centrifugation and rinsed several times with ethanol. Si MLs (100 mg) were mixed with 200 mM of CsBr and PbBr $_2$ with 1:1 mol ratio in DMSO overnight at room temperature. The product was separated by centrifugation at 2000 rpm and placed in a filter paper, which was baked at 95 $^{\circ}$ C for 30 min. Finally, the sample was kept in vacuum until further use.

For comparison, the bulk material, 1 drop of the solution of 200 mM of CsBr and PbBr₂ with 1:1 mol ratio in DMSO, was placed on the substrate and baked for 30 min at 95 °C.

Device Fabrication and Characterization. The fabrication of a typical LED device involves spin-coating of PEDOT:PSS on an FTO glass at 3000 rpm for 40 s, followed by baking at 120 °C for 15 min. The sample was then kept overnight in a vacuum oven. The quantum-confined CsPbBr₃ in silicene was deposited by the drop cast method, which involves the dispersion of the confined CsPbBr₃ in toluene, by placing 20 μ L on the FTO-PEDOT:PSS, drying in vacuum, depositing Ag paste in contact with a working area of 0.15 cm², and finally curing at 95 °C for 15 min. The electrical properties were characterized using a Keithley 4200 semiconductor analyzer. The emission power was measured by a power meter and used to calculate the number of emitted photons with the given wavelength. The current at a given voltage was used to calculate the injected electrons so that the EQE was obtained by using the ratio of emitted photons to the injected electrons.

ASSOCIATED CONTENT

Supporting Information

The Supporting Information is available free of charge at https://pubs.acs.org/doi/10.1021/acsanm.3c00404.

XRD patterns, SEM images, absorption spectrum, PL emission spectrum, PL tracking, EL emission spectrum, QE% vs current density plots, EL stability measurement, and PL lifetime measurement (PDF)

AUTHOR INFORMATION

Corresponding Author

Jingbiao Cui — Department of Physics, University of North Texas, Denton, Texas 76203, United States; oorcid.org/0000-0003-3408-1016; Email: jingbiao.cui@unt.edu

Authors

Roberto Gonzalez-Rodriguez — Department of Physics, University of North Texas, Denton, Texas 76203, United States; Occid.org/0000-0001-6849-1799

Evan Hathaway – Department of Physics, University of North Texas, Denton, Texas 76203, United States

Holden Paulette – Department of Physics, University of North Texas, Denton, Texas 76203, United States

Jeffery L. Coffer – Department of Chemistry and Biochemistry, Texas Christian University, Fort Worth, Texas 76129, United States; orcid.org/0000-0003-0267-9646

Yuankun Lin – Department of Physics, University of North Texas, Denton, Texas 76203, United States

Complete contact information is available at: https://pubs.acs.org/10.1021/acsanm.3c00404

Notes

The authors declare no competing financial interest.

ACKNOWLEDGMENTS

This work was supported by the U.S. National Science Foundation (#2128367).

REFERENCES

- (1) Oga, H.; Saeki, A.; Ogomi, Y.; Hayase, S.; Seki, S. Improved Understanding of the Electronic and Energetic Landscapes of Perovskite Solar Cells: High Local Charge Carrier Mobility, Reduced Recombination, and Extremely Shallow Traps. *J. Am. Chem. Soc.* **2014**, *136*, 13818–13825.
- (2) Xing, G.; Mathews, N.; Sun, S.; Lim, S. S.; Lam, Y. M.; Grätzel, M.; Mhaisalkar, S.; Sum, T. C. Long-Range Balanced Electron- and Hole-Transport Lengths in Organic-Inorganic CH₃NH₃PbI₃. *Science* **2013**, 342, 344–347.
- (3) Rathore, E.; Maji, K.; Rao, D.; Saha, B.; Biswas, K. Charge Transfer in the Heterostructure of CsPbBr₃ Nanocrystals with Nitrogen-Doped Carbon Dots. *J. Phys. Chem. Lett.* **2020**, *11*, 8002–8007.
- (4) Rathore, E.; Kundu, K.; Maji, K.; Das, A.; Biswas, K. Mixed-Dimensional Heterostructure of $CsPbBr_3$ Nanocrystal and Bi_2O_2Se Nanosheet. *J. Phys. Chem. C* **2021**, *125*, 26951–26957.
- (5) Juarez-Perez, E. J.; Sanchez, R. S.; Badia, L.; Garcia-Belmonte, G.; Kang, Y. S.; Mora-Sero, I.; Bisquert, J. Photoinduced Giant Dielectric Constant in Lead Halide Perovskite Solar Cells. *J. Phys. Chem. Lett.* **2014**, *5*, 2390–2394.
- (6) Zhang, M.; Zhang, F.; Wang, Y.; Zhu, L.; Hu, Y.; Lou, Z.; Hou, Y.; Teng, F. High-Performance Photodiode-Type Photodetectors Based on Polycrystalline Formamidinium Lead Iodide Perovskite Thin Films. *Sci. Rep.* **2018**, *8*, 11157.
- (7) Fu, F.; Feurer, T.; Weiss, T. P.; Pisoni, S.; Avancini, E.; Andres, C.; Buecheler, S.; Tiwari, A. N. High-efficiency inverted semi-transparent planar perovskite solar cells in substrate configuration. *Nat. Energy* **2017**, *2*, 16190.
- (8) He, X.; Liu, P.; Wu, S.; Liao, Q.; Yao, J.; Fu, H. Multi-color perovskite nanowire lasers through kinetically controlled solution growth followed by gas-phase halide exchange. *J. Mater. Chem. C* **2017**, *5*, 12707–12713.
- (9) Wang, H.; Zhang, X.; Wu, Q.; Cao, F.; Yang, D.; Shang, Y.; Ning, Z.; Zhang, W.; Zheng, W.; Yan, Y.; Kershaw, S. V.; Zhang, L.; Rogach, A. L.; Yang, X. Trifluoroacetate induced small-grained

- CsPbBr₃ perovskite films result in efficient and stable light-emitting devices. *Nat. Commun.* **2019**, *10*, 665.
- (10) Stoumpos, C. C.; Cao, D. H.; Clark, D. J.; Young, J.; Rondinelli, J. M.; Jang, J. I.; Hupp, J. T.; Kanatzidis, M. G. Ruddlesden—Popper Hybrid Lead Iodide Perovskite 2D Homologous Semiconductors. *Chem. Mater.* **2016**, *28*, 2852–2867.
- (11) Ishihara, T.; Takahashi, J.; Goto, T. Exciton state in two-dimensional perovskite semiconductor $(C_{10}H_{21}NH_3)_2PbI_4$. *Solid State Commun.* **1989**, *69*, 933–936.
- (12) Quan, L. N.; García de Arquer, F. P.; Sabatini, R. P.; Sargent, E. H. Perovskites for Light Emission. *Adv. Mater.* **2018**, *30*, No. 1801996.
- (13) Calabrese, J.; Jones, N. L.; Harlow, R. L.; Herron, N.; Thorn, D. L.; Wang, Y. Preparation and characterization of layered lead halide compounds. *J. Am. Chem. Soc.* **1991**, *113*, 2328–2330.
- (14) Mitzi, D. B. Synthesis, Crystal Structure, and Optical and Thermal Properties of $(C_4H_9NH_3)_2MI_4$ (M = Ge, Sn, Pb). Chem. Mater. 1996, 8, 791–800.
- (15) Kataoka, T.; Kondo, T.; Ito, R.; Sasaki, S.; Uchida, K.; Miura, N. Magneto-optical study on excitonic spectra in $(C_6H_{13}NH_3)_2PbI_4$. *Phys. Rev. B* **1993**, 47, 2010–2018.
- (16) Muljarov, E. A.; Tikhodeev, S. G.; Gippius, N. A.; Ishihara, T. Excitons in self-organized semiconductor/insulator superlattices: PbI-based perovskite compounds. *Phys. Rev. B* **1995**, *51*, 14370–14378.
- (17) Ahmad, S.; Fu, P.; Yu, S.; Yang, Q.; Liu, X.; Wang, X.; Wang, X.; Guo, X.; Li, C. Dion-Jacobson Phase 2D Layered Perovskites for Solar Cells with Ultrahigh Stability. *Joule* **2019**, *3*, 794–806.
- (18) Gonzalez-Rodriguez, R.; del Castillo, R. M.; Hathaway, E.; Lin, Y.; Coffer, J. L.; Cui, J. Silicene/Silicene Oxide Nanosheets for Broadband Photodetectors. *ACS Appl. Nano Mater.* **2022**, *5*, 4325–4335.
- (19) Ramachandran, R.; Leng, X.; Zhao, C.; Xu, Z.-X.; Wang, F. 2D siloxene sheets: A novel electrochemical sensor for selective dopamine detection. *Appl. Mater. Today* **2020**, *18*, No. 100477.
- (20) Dahn, J. R.; Way, B. M.; Fuller, E.; Tse, J. S. Structure of siloxene and layered polysilane (Si₆H₆). *Phys. Rev. B* **1993**, 48, 17872–17877.
- (21) Chen, W.; Xin, X.; Zang, Z.; Tang, X.; Li, C.; Hu, W.; Zhou, M.; Du, J. Tunable photoluminescence of CsPbBr3 perovskite quantum dots for light emitting diodes application. *J. Solid State Chem.* **2017**, 255, 115–120.
- (22) Rakita, Y.; Kedem, N.; Gupta, S.; Sadhanala, A.; Kalchenko, V.; Böhm, M. L.; Kulbak, M.; Friend, R. H.; Cahen, D.; Hodes, G. Low-Temperature Solution-Grown CsPbBr₃ Single Crystals and Their Characterization. *Cryst. Growth Des.* **2016**, *16*, 5717–5725.
- (23) Parrott, E. S.; Patel, J. B.; Haghighirad, A.-A.; Snaith, H. J.; Johnston, M. B.; Herz, L. M. Growth modes and quantum confinement in ultrathin vapour-deposited MAPbI3 films. *Nanoscale* **2019**, *11*, 14276–14284.
- (24) Protesescu, L.; Yakunin, S.; Bodnarchuk, M. I.; Krieg, F.; Caputo, R.; Hendon, C. H.; Yang, R. X.; Walsh, A.; Kovalenko, M. V. Nanocrystals of Cesium Lead Halide Perovskites (CsPbX₃, X = Cl, Br, and I): Novel Optoelectronic Materials Showing Bright Emission with Wide Color Gamut. *Nano Lett.* **2015**, *15*, 3692–3696.
- (25) Maity, G.; Pradhan, S. K. Composition related structural transition between mechanosynthesized CsPbBr3 and CsPb2Br5 perovskites and their optical properties. *J. Alloys Compd.* **2020**, *816*, No. 152612.
- (26) Liu, M.; Zhao, J.; Luo, Z.; Sun, Z.; Pan, N.; Ding, H.; Wang, X. Unveiling Solvent-Related Effect on Phase Transformations in CsBr–PbBr₂ System: Coordination and Ratio of Precursors. *Chem. Mater.* **2018**, *30*, 5846–5852.
- (27) Paul, T.; Sarkar, P. K.; Maiti, S.; Sahoo, A.; Chattopadhyay, K. K. Solution-processed light-induced multilevel non-volatile wearable memory device based on CsPb2Br₅ perovskite. *Dalton Trans.* **2022**, *51*, 3864–3874.
- (28) Murugadoss, G.; Thangamuthu, R.; Senthil Kumar, S. M.; Anandhan, N.; Rajesh Kumar, M.; Rathishkumar, A. Synthesis of ligand-free, large scale with high quality all-inorganic $CsPbI_3$ and

- CsPb2Br₅ nanocrystals and fabrication of all-inorganic perovskite solar cells. *J. Alloys Compd.* **2019**, *787*, 17–26.
- (29) Gotanda, T.; Kimata, H.; Xue, D.; Asai, H.; Shimazaki, A.; Wakamiya, A.; Marumoto, K. Direct observation of charge transfer at the interface between PEDOT:PSS and perovskite layers. *Appl. Phys. Express* **2019**, *12*, No. 041002.
- (30) Cheng, X.; Qi, C.; Ding, W.; Lu, J.; Mo, X.; Zhou, Y.; Lin, T.; Tao, X.; Chen, H.; Ouyang, Y. Boosted electroluminescence of perovskite light-emitting diodes by pinhole passivation with insulating polymer. *J. Phys. D: Appl. Phys.* **2018**, *51*, No. 405103.
- (31) Miao, Y.; Cheng, L.; Zou, W.; Gu, L.; Zhang, J.; Guo, Q.; Peng, Q.; Xu, M.; He, Y.; Zhang, S.; Cao, Y.; Li, R.; Wang, N.; Huang, W.; Wang, J. Microcavity top-emission perovskite light-emitting diodes. *Light: Sci. Appl.* **2020**, *9*, 89.
- (32) Zhang, X.; Wang, H.-C.; Tang, A.-C.; Lin, S.-Y.; Tong, H.-C.; Chen, C.-Y.; Lee, Y.-C.; Tsai, T.-L.; Liu, R.-S. Robust and Stable Narrow-Band Green Emitter: An Option for Advanced Wide-Color-Gamut Backlight Display. *Chem. Mater.* **2016**, 28, 8493–8497.
- (33) Lou, S.; Xuan, T.; Yu, C.; Cao, M.; Xia, C.; Wang, J.; Li, H. Nanocomposites of CsPbBr3 perovskite nanocrystals in an ammonium bromide framework with enhanced stability. *J. Mater. Chem. C* **2017**, *5*, 7431–7435.
- (34) Wang, R.; Jia, Y.-L.; Ding, L.; He, Z.; Dong, Y.; Ma, X.-J.; Zhang, Y.; Zhou, D.-Y.; Zhu, Z.-X.; Xiong, Z.-H.; Gao, C. H. Efficient halide perovskite light-emitting diodes with emissive layer consisted of multilayer coatings. *J. Appl. Phys.* **2019**, *126*, No. 165502.
- (35) Zou, Y.; Ban, M.; Yang, Y.; Bai, S.; Wu, C.; Han, Y.; Wu, T.; Tan, Y.; Huang, Q.; Gao, X.; Song, T.; Zhang, Q.; Sun, B. Boosting Perovskite Light-Emitting Diode Performance via Tailoring Interfacial Contact. ACS Appl. Mater. Interfaces 2018, 10, 24320–24326.
- (36) Quan, L. N.; Zhao, Y.; García de Arquer, F. P.; Sabatini, R.; Walters, G.; Voznyy, O.; Comin, R.; Li, Y.; Fan, J. Z.; Tan, H.; Pan, J.; Yuan, M.; Bakr, O. M.; Lu, Z.; Kim, D. H.; Sargent, E. H. Tailoring the Energy Landscape in Quasi-2D Halide Perovskites Enables Efficient Green-Light Emission. *Nano Lett.* **2017**, *17*, 3701–3709.
- (37) Chen, Z.; Zhang, C.; Jiang, X.-F.; Liu, M.; Xia, R.; Shi, T.; Chen, D.; Xue, Q.; Zhao, Y.-J.; Su, S.; Yip, H. L.; Cao, Y. High-Performance Color-Tunable Perovskite Light Emitting Devices through Structural Modulation from Bulk to Layered Film. *Adv. Mater.* **2017**, 29, No. 1603157.
- (38) Warby, J. H.; Wenger, B.; Ramadan, A. J.; Oliver, R. D. J.; Sansom, H. C.; Marshall, A. R.; Snaith, H. J. Revealing Factors Influencing the Operational Stability of Perovskite Light-Emitting Diodes. *ACS Nano* **2020**, *14*, 8855–8865.
- (39) Chen, P.; Meng, Y.; Ahmadi, M.; Peng, Q.; Gao, C.; Xu, L.; Shao, M.; Xiong, Z.; Hu, B. Charge-transfer versus energy-transfer in quasi-2D perovskite light-emitting diodes. *Nano Energy* **2018**, *50*, 615–622.
- (40) Lee, S.; Kim, D. B.; Hamilton, I.; Daboczi, M.; Nam, Y. S.; Lee, B. R.; Zhao, B.; Jang, C. H.; Friend, R. H.; Kim, J.-S.; Song, M. H. Control of Interface Defects for Efficient and Stable Quasi-2D Perovskite Light-Emitting Diodes Using Nickel Oxide Hole Injection Layer. *Adv. Sci.* 2018, 5, No. 1801350.
- (41) Kumar, S.; Jagielski, J.; Yakunin, S.; Rice, P.; Chiu, Y.-C.; Wang, M.; Nedelcu, G.; Kim, Y.; Lin, S.; Santos, E. J. G.; Kovalenko, M. V.; Shih, C. J. Efficient Blue Electroluminescence Using Quantum-Confined Two-Dimensional Perovskites. *ACS Nano* **2016**, *10*, 9720–9729.